IRSO-1963

EA-6010-21
Dist. Category UC-90C

MATERIALS RESEARCH FOR THE CLEAN UTILIZATION OF COAL

QUARTERLY PROGRESS REPORT

July - September 1979

Samuel J. Schneider
Project Manager

Center for Materials Science
National Bureau of Standards
Washington, D.C. 20234

PREPARED FOR THE UNITED STATES
DEPARTMENT OF ENERGY

Under Contract No. EA-77-A-01-6010

TABLE OF CONTENTS

I. OBJECTIVE AND SCOPE OF WORK

Coal gasification and other conversion processes require the handling and containment of corrosive gases and liquids at high temperature and pressures, and also the handling of flowing coal particles in these environments. These severe environments cause materials failures which inhibit successful and long-time operation. The project entails investigations on the wear, corrosion, chemical and electrical degradation, fracture, and deformation processes which lead to the breakdown of metals and ceramics currently being utilized in test facilities and pilot plants. Studies will also be carried out on new candidate materials considered for improved performance. Special emphasis will be devoted to the development of test methods, especially short-time procedures, to evaluate the durability of materials in the severe environments. These methods will focus on wear, impact erosion, stress corrosion, strength, deformation, slow crack growth and chemical degradation. A system has been initiated to abstract and compile all significant operating incidents from coal conversion plants as well as materials property and performance information important to the design and operation of these plants. This program will provide a central information center where probblems of common interest can be identified and analyzed to avoid unnecessary failures and lead to the selection of improved materials for coal conversion and utilization. Active consultation to DOE and associated contractors will be provided as requested.

II. SUMMARY OF PROGRESS TO DATE

Brief Summary

1. Metal Corrosion

a. Pre-Cracked Fracture Test: Experimental verification of the analysis for the change in stress-intensity ratio (K_T/K_o) with temperaature was conducted for the tension-loaded DCB specimen. These tests showed that the stress-intensity change with temperature is very sensitive to the thermal expansion of the loading fixture. The stress-intensity can be made to increase substantially with temperature.

2. Ceramic Deformation, Fracture, and Erosion

The earlier part of this quarter was spent making repairs to the apparatus for mechanical testing at elevated pressure and temperature. Following these repairs, a series of experiments was begun on newly formulated batches of an intermediate-alumina (56%) refractory concrete. These experiments involved an *in situ* measurement of the modulus of rupture following a 70 hour hydrothermal exposure. In addition, the porosity and pore size distribution were measured for two intermediate-alumina (50% and 56%) refractory concretes to examine the influence of these properties on the modulus of rupture. Two additional experiments are planned with the mechanical testing apparatus at elevated pressure and temperature to complete the studies begun this quarter. Upon completion of these experiments and analysis of the data, the final report will be prepared.

3. Chemical Degradation

a. Reactions and Transformations

Additional data has been obtained on the behavior of CA_2 and CA_6 in hydrothermal environments.

Preparation of a final report summarizing the work of this task is in progress.

b. Slag Characterization

As discussed in previous reports, it was decided to measure the viscosity of the melt while extending its temperature to the maximum achievable with the existing platinum heater until burn out occurred. At this point a new heater would be constructed from 60% Pt-40% Rh to increase the melt temperature. The melt which is currently being investigated has the following composition: SiO_2, 48.30%; Al_2O_3, 12.10%; Fe_2O_3, 12.00%; CaO, 14.90; MgO, 8.00%; and Na_2O, 4.70% (wt%).

Five experiments were conducted and each resulted in slag spills and/or heater burn outs resulting in extensive rebuilding of the viscometer vessel internals.

c. Vaporization and Chemical Transport

Vapor transport data, in the form of alkali species partial pressures, have been obtained for the K_2 slag system, of initial composition (wt%) SiO_2 47.3, Al_2O_3 11.1, Fe_2O_3 12, CaO 13.9, MgO 7.8 and K_2O 8.7, using the transpiration mass spectrometric technique (TMS). Complementary computer modeling calculations, using the SOLGASMIX program, have also been made. Data obtained previously for the so-called K_1 slag, of initial composition (wt.%) Al_2O_3 12.06, CaO 3.8, Cr_2O_3 1.3, Fe_2O_3 14.25, K_2O 19.54, MgO 1.03, Na_2O 0.47, SO_3 0.21, SiO_2 46.82, and TiO_2 0.52, have been analyzed, and presented at an international symposium.

4. Failure prevention

a. Failure Information Center

Five additional reports of operating experiences and failure analysis were entered into the Center's data base. Approximately 2,800 information items were distributed to DoE contractors and newsletter readers during this quarter. A draft report on erosive wear failures was completed and a feature article for the Materials and Components Newsletter was submitted for publication in the October, 1979 issue.

b. Materials Properties Data Center

The routine on-going data tasks of the Center have continued during the quarter. A major emphasis has been the effort to expedite the acquisition of computer vendors' services through contacts with the DOC ADP procurement division, the vendors who have submitted proposals and the preparation of benchmark test material.

5. Creep of MHD Refractories

Efforts this quarter were directed toward obtaining data on the deformation of the chrome-iron spinel refractory. The reduced cross-section type of creep specimen was evaluated in creep tests at 1400, 1500 and 1600°C. The material was characterized using X-ray diffraction, light microscopy and scanning electron microscopy. The results are reported in the text.

6. Electrical Transport Mechanisms in Slag Associated with Electrochemical Degradation of Insulator and Electrode Materials

The measurement of the electrical conductivity of $YCrO_3$ (.05 Ca) as a function of oxygen pressure from 10^0 to 10^{-15} atmospheres has been started. Some difficulty has been encountered in the low pressure regions because of hydrogen embrittlement of the platinum electrode leadouts.

The analytical work on the electrochemical corrosion at 1343°C of $YCrO_3$ in Bow NH slag with 20% K_2SO_4 added has been completed. While the cathode showed a sizeable attack zone, the anode attack zone was small. The total reaction layer was about .03mm thick composed of a boundary layer of Fe-Cr-Al spinel without Si and a zone near the undisturbed electrode material composed of Fe-Cr-Al spinel but rich in silicon.

The electrical conductivity as a function of temperature of Bow NH slag with 20% K_2SO_4 added to the melt has been completed. These measurements were done in air and at a reduced oxygen pressure but the latter run must be repeated because of an experimental difficulty. Just as in the measurements of the Bow NH slag without the K_2SO_4 added, this slag was quenched from a higher soak temperature to below the softening point in order to quench in the Fe^{+2}/Fe^{+3} ratio established at the higher temperature. The two materials (with and without K_2SO_4) behave quite differently, the latter showing a large ionic current down to low temperature.

7. Corrosion of Downstream MHD Components

Type 304 stainless steel tubes, maintained at 400°C, 500°C, and 590°C were exposed to K_2SO_4 seeded fuel rich and oxygen rich hot gas streams. Optical and SEM examinations and EDX analysis of the specimens revealed differences in the deposits formed on the tubing (thinner in the fuel rich stream) as well as differences in nickel distribution in the reaction zone of the metal-deposit interface. In the coming quarter, a similar series will be run but with a mixture of 80% by weight K_2CO_3 and 20% by weight K_2SO_4 added to the hot gas stream.

Articles Published and Talks Presented

R. C. Dobbyn, "How do we handle the Subjective Component of Inservice Data Reporting and Analysis", ASME, Materials and Fabrication Committee Meeting, San Antonio, Aug 1979.

W. S. Brower, R. C. Dobbyn, and C. R. Robbins, "Refractory CO_2 Acceptor Gasifier Lining Reviewed", DOE Materials and Components Newsletter, October, 1979.

II. DETAILED DESCRIPTION OF TECHNICAL PROGRESS

1. Metal Corrosion

a. Pre-Cracked Fracture Test (J. H. Smith and G. E. Hicho, 562)

Progress: Tests were continued to experimentally verify the analysis for the change in stress-intensity ratio (K_T/K_Q) with temperature for the tension-loaded DCB specimen. The loading fixture used was made of type 347 stainless steel and the specimen grips were made of Inconel 600. Measurement of the increase in load-line displacement, V, with temperature were made with a linear-voltage displacement transducer (LVDT). Measurement of the load-line displacement were made at temperatures from 0 to 500°C.

Previous results indicated that a discrepancy existed between the measured change in load-line displacement with temperature and the change in displacement calculated from the differences in thermal expansion of the loading fixture and loading grips. This discrepancy may result from 1) unexpected variation in the thermal expansion of the specimen and loading fixture and 2) errors associated with translating displacements measured on the edge of the specimen to the displacement at the load-line position. Experiments were conducted to assess the magnitude of these two sources of error.

The loading fixture was modified to permit direct measurement of the displacement at the loading position for the specimen. Measurements were then performed with the specimen removed from the loading fixture to assess changes in the length of the test fixture and loading grips with temperature. These measurements showed that the thermal expansion of the test fixture was significantly larger than originally calculated. This means that the loading fixture as designed would be over compensating, that is, would cause the stress intensity, K_T, to increase with temperature, rather than remained constant as required.

A sensitivity analysis indicated that the larger than anticipated thermal expansion described above, may arise from small variations in the amount of thermal expansion occurring in the loading fixture. Small variations in the thermal expansion of the loading fixture and loading grips may result in significant variations in the displacement of the test specimen with temperature.

The discrepancy between the measured and expected load-line displacement due to translation of the displacement measurements from the specimen to the load-line were assessed by measuring the displacements at both points on the test specimens. These results showed that the usual procedure of using the method of similar triangles to make this required measurement translation did not result in significant errors.

Plans: Work on this research project is now discontinued and there are no plans for further work.

2. Ceramic Deformation, Fracture, and Erosion (E. R. Fuller, Jr., S. M. Wiederhorn, D. E. Roberts, and L. Chuck, 562)

Progress: The earlier part of this quarter was spent making repairs to the apparatus for mechanical testing at elevated pressure and temperature. Following these repairs, a series of experiments was begun on newly formulated batches of an intermediate-alumina (56%) refractory concrete. These experiments involved an *in situ* measurement of the modulus of rupture following a 70 hour hydrothermal exposure. In addition, the porosity and pore size distribution were measured for two intermediate-alumina (50% and 56%) refractory concretes to examine the influence of these properties on the modulus of rupture. These studies are described below.

At the end of last quarter, while testing the high-alumina refractory concrete at a temperature of 1010°C and a steam pressure of 1100 psia, a segment of the lower heater in our main furnace burned out. To replace this heater segment, the apparatus had to be disassembled and the lower furnace assembly had to be completely rebuilt. While the apparatus was disassembled for these repairs, a number of other minor repairs were undertaken: the subheater surrounding the lower loading bellows was replaced with a larger wattage heater; new gaskets were installed in the lower flange of the inner environmental chamber; and the steel bolts previously used in this flange were replaced with stainless steel bolts to match better the thermal expansion of the flange. Towards the end of the quarter, the system was again disassembled to replace the lower loading bellows which had developed several pin-hole size leaks.

Following the repairs to the furnace assembly, a series of experiments was begun on newly formulated batches of an intermediate-alumina (56%) refractory concrete. The exposure conditions for these experiments were similar to those used last quarter for the high-alumina refractory. The specimens were exposed at temperature and pressure to steam for at least 70 hours prior to an *in situ* measurement of the modulus of rupture. Additional specimens were simultaneously exposed to the same environment; but they were then cooled to room temperature and atmospheric pressure before they were broken to determine their modulus of rupture. Experiments thus far have been conducted at steam pressures of nominally 800 to 1000 psia and at temperatures of 360°C and 1010°C. The experiment at 660°C will be conducted next quarter.

In addition to these experiments, the influence of porosity and pore size distribution on the modulus of rupture was examined for two intermediate-alumina refractory concretes. A mercury porosimeter was used to determine the open pore porosity and size distribution both in control specimens and in specimens that had been exposed to hydrothermal conditions. The hydrothermally exposed, and stronger, specimens had a greater porosity than the control specimens, but the pore size distribution was skewed towards smaller pore sizes.

Plans: Two additional experiments are presently planned. The first experiment is to complete the series of *in situ* modulus-of-rupture experiments on the intermediate alumina refractory concrete with a test at 660°C. Time permitting, the high-alumina refractory concrete will be tested in a simulated coal gasification environment at a temperature of 1010°C and a total pressure of 1000 psia (6.9 MPa). Following completion of these experiments and analysis of the data, the final report will be prepared.

3. Chemical Degradation

a. Reactions and Transformations (F. A. Mauer and C. R. Robbins, 565)

Progress: Analysis of forty *in situ* x-ray patterns of a test bar of CA_2** exposed to high pressure steam, and to a steam - carbon dioxide atmosphere has been completed.

A test bar of CA_6 has been exposed to steam at 300°C (220 psig*) for 700 hours. This compound with the ß-A structure forms readily at 1400°C in air but its stability under low temperature hydrothermal conditions is not clear. Small amounts of ß-A are commonly encountered in hydrothermal exposure tests of high purity castables, but with compositions other than that of pure CA_6.

Several tests bars of high and low Al_2O_3 content refractory castables from the exposure tests of Task 2 were examined by conventional x-ray diffraction methods.

All experimental data obtained during the *in situ* x-ray study of Task 3, the x-ray characterization study of Task 2 specimens, and the light microscope, SEM and x-ray diffraction analyses of core samples from the refractory lining of the Conoco Lignite Gasification Pilot Plant gasifier have been reviewed and correlated. Preparation of a summary report is in progress.

Plans: A final report summarizing the work of this task will be prepared.

b. Slag Characterization (W. S. Brower, J. L. Waring, and D. H. Blackburn, 565)

Progress: As discussed previously, it was decided to measure the viscosity of the melt while extending its temperature to the maximum achievable with the existing platinum heater until burn out occurred. At this point a new heater would be constructed from 60%Pt-40%Rh to increase the melt temperature. The melt which is currently being investigated has the following composition: SiO_2, 48.30%; Al_2O_3, 12.10%; Fe_2O_3, 12.00%; CaO, 14.90%; MgO, 8.00%; and Na_2O, 4.70% (wt%).

* In SI unit, 1 MPa = 145 psia.
** Cement notation
C = CaO
A = Al_2O_3

In the first experiment prior to measuring viscosity, the platinum heater was operating at about 1511°C at ambient pressure. The viscosity bob-thermocouple assembly was introduced into the melt. The temperature of the melt was 1386°C which is well within the fluid range of the composition. The physical position of the bob is not visible and can only be approximated at these elevated temperatures. Prior to generating steam pressure, the viscosity at ambient pressure is usually checked. However, when the crucible containing the melt was rotated no angular deflection was detected on the magnetic position detector and the experiment was terminated. Figure 1 shows the after-the-fact physical picture of the failure. From the above it can be seen that the platinum crucible was lifted from the pedestal and welded to the platinum heater.

Catastrophic failures result in the loss of many weeks since it is necessary to rebuild the platinum crucible, remake the ceramic pedestal, reshape the platinum heater, rebuild and recalibrate the suspension.

Since it was thought that the bob was inadvertently introduced into the liquid, experiment one was duplicated in experiment two. The results were similar but not as disastrous. The crucible welded to the heater but the suspension remained intact.

In experiment three the slag was melted out of the vessel in air and the melt was observed. In the melting process the center of the melt (coldest portion) remained solid and as the edges melted the resulting liquid foamed up the sides and out of the crucible. When a platinum rod positioned above the surface of the liquid came into contact with the foaming material the rod served to bridge and extract all of the liquid from the crucible. In experiment one, the foaming liquid probably pushed the bob to the side where it welded to the crucible after which, when the pedestal was rotated, the crucible was lifted from the pedestal and welded to the heater.

This foaming problem is probably due to evolution of oxygen gas as Fe^{+3} is converted to Fe^{+2} on heating. From additional experimentation it was found that the foaming problem could be eliminated by annealing the starting melt at 1500°C for 4 hrs before placing it into the viscometer.

In experiment four, a new batch of material previously heated as described above was placed in the viscometer for viscosity measurements. The platinum heater was controlling properly at 1420°C but burned out prior to the introduction of the viscosity measuring bob. From figure 1 it can be seen that the burn out pattern on the platinum cylinder is near the position where the platinum electrode fin had been welded to the heater. In the design the position of the electrodes are fixed therefore fixing the platinum fins which are clamped to the electrodes. Thus, thermal expansion is accomplished by changes in the geometry of the platinum heater cylinder. It is most likely that the platinum was "work hardened" by repeated movement caused by such geometry changes and burned out where the metal endured maximum flexing.

Figure 1. Burn out pattern of the platinum heater.

These massive fins were removed from the cylinder and were welded to a new cylinder of 60%Pt and 40%Rh. Two layers of insulating material were cast about the heater. The inner layer was fabricated from green cast 97 and the outer layer from VSL 50.

In experiment five the 60%Pt-40%Rh heater was heated to 1480°C. The doughnut shaped lid was removed for greater visibility of the melt. The material maintained at the temperature for several hours was visually observed to be melted. The bob was observed continuously as it was lowered 1/4" at a time into the melt. At or near the surface of the liquid the bob shifted position and welded to the side of the crucible, which in turn welded to the 60/40 heater. The run was terminated.

Plans: The 60% platinum 40% rhodium heater will be used in an attempt to obtain viscosity at higher temperatures than those obtainable with the pure platinum heater.

c. Vaporization and Chemical Transport (J. Hastie, D. Bonnell and W. Horton)

Progress: Vapor transport data, in the form of alkali species partial pressures, have been obtained for the K_2 slag system, of initial composition (wt%) SiO_2 47.3, Al_2O_3 11.1, Fe_2O_3 12, CaO 13.9, MgO 7.8 and K_2O 8.7, the transpiration mass spectrometric technique (TMS). Complementary computer modeling calculations, using the SOLGASMIX program, have also been made. Data obtained previously for the so-called K_1 slag, of initial composition (wt.%) Al_2O_3 12.06, CaO 3.8, Cr_2O_3 1.3, Fe_2O_3 14.25, K_2O 19.54, MgO 1.03, Na_2O 0.47, SO_3 0.21, SiO_2 46.82, and TiO_2 0.52, have been analyzed, and presented at an international symposium.

1. $K_2 + H_2$ Slag-Gas System:

In the previous Quarterly Report (PQR), we presented vapor transport data for the K_2 synthetic slag (approximates an alkali enriched "Western-type" basic slag) as a function of temperature and H_2O partial pressure. Both these variables had a strong effect on the rate of vaporization of K_2O from the slag, primarily in the form of K and O_2 species. For instance, an 100 K increase in temperature, or a two order of magnitude increase in H_2O pressure, led to about an order of magnitude increase in slag vapor pressure, e.g., see Figs. 3 and 4 of PQR, respectively. The most significant reactions giving rise to these dependences are considered to be

$$K_2O\ (\ell)\ (\text{in slag}) = 2K + 1/2\ O_2 \qquad (1)$$

$$K_2O\ (\ell)\ (\text{in slag}) + H_2 = 2K + H_2O \qquad (2)$$

$$H_2O = H_2 + 1/2\ O_2. \qquad (3)$$

Also, relatively insignificant amounts of KOH were formed under these conditions. In order to verify this reaction scheme, and to extend the vapor transport conditions to reducing conditions close to those present in coal gas, a series of measurements were made using H_2 as the initial reactant gas. Compositions of H_2-N_2-H_2O-O_2 gas up to 10 volume % H_2 were attained prior to corrosive loss of the transpiration reactor.

As H_2 is introduced to the slag system the O_2 concentration is decreased and H_2O increases in accord with reaction (3). Typical data are given in Fig. 1. Note that at relatively low H_2 concentration ($< 5x10^{-3}$ atm) the O_2 scavenging process provides a high concentration of H_2O. As there are three interdependent (through reactions (1)-(3)) reactive gases simultaneously present; namely, H_2, H_2O and O_2, the dependence of K pressure on reactive gas pressure can be complex, as shown in Fig. 2. For the decreasing pressure region of the run chronology, the one-half power dependence of K pressure on H_2O pressure (resulting from reaction (3)) is consistent with reactions (2) and (3).

2. K_2 Slag System--Time Dependent Observations:

During the initial heating-vaporization phase, using a non-reactive N_2 carrier gas, a periodic pressure burst phenomenon was noted for both the K and O_2 vapor species. As shown in Fig. 3, the rise time for such a burst is almost instantaneous once the critical temperature is reached. After about 20 min., at constant temperature, the K and O_2 pressures return to the expected level. This type of phenomenon has also recently been observed in solar heating experiments of liquid oxides. The explanation for this effect in our system is unclear but may be indicative of a non-homogeneous sample, perhaps containing residual K_2CO_3 used in the slag-synthesis. Alternatively, phase separation of an initially homogeneous sample may be possible.

A second type of time dependent phenomenon was observed for this slag, as shown in Fig. 4. Once an isothermal condition has been achieved the K pressure falls off with time. We believe that this results from surface depletion of K (and O_2) from the sample due to the bulk rate of diffusion being too small relative to the surface vaporization rate. This effect was found to be much less pronounced at higher temperatures where the diffusion rates are probably higher.

3. Modeling of the $K_2 + H_2$ Slag-Gas Systems:

An equilibrium model has been chosen to describe the chemical interaction between gaseous environment and coal slag. To utilize the model fully requires a knowledge of activity coefficients of the slag constituents which may contribute to chemical interaction with the gas. Also required is a computer program which gives equilibrium compositions for systems containing not only a gaseous phase and pure condensed phases but also solutions that are not ideal. A start on the problem of the activity coefficient of K_2O in slag has been made using vapor pressure data obtained in this laboratory for K_2O-SiO_2 solutions. Redlich-Kister type equations have been developed and a choice among these has to be made. A program known as SOLGASMIX, developed at the University of Umeå, Sweden, has been received which handles the required systems described above. It will solve both constant pressure and constant volume problems at fixed temperature. To use the non-ideal solution feature, an equation for the activity coefficient of a species is needed. This will usually be a function of mole fraction and temperature. A few trial runs of the program have been made.

Typical output data obtained from the SOLGASMIX program for the K_2 slag in the presence of H_2 are given in table 1. Note that K is the predominant alkali vapor species, in agreement with experimental observation. However, the O_2 partial pressures are much less than observed experimentally. It is also noteworthy that the K partial pressure is relatively temperature insensitive in the presence of H_2 and H_2O. This agrees qualitatively with data presented in the previous Quarterly Report for the K_1 slag system (e.g., see Fig. 1 of previous report).

Table 1

Species partial pressures from non-ideal solution[a] multicomponent equilibrium calculations for K_2 slag + H_2

Species	Pressure (atm) (1600 K)		Pressure (atm) (1700 K)	
H_2	0.11	-3[b]	0.63	-4
H_2O	0.26	-3	0.27	-3
O_2	0.23	-9	0.77	-8
K	0.57	-3	0.60	-3
KOH	0.51	-4	0.55	-4
SiO	0.54	-8	0.31	-7

[a] K_2O activity coefficient specified as 10^{-8} and independent of temperature.

[b] Denotes e.g., 0.11×10^{-3}

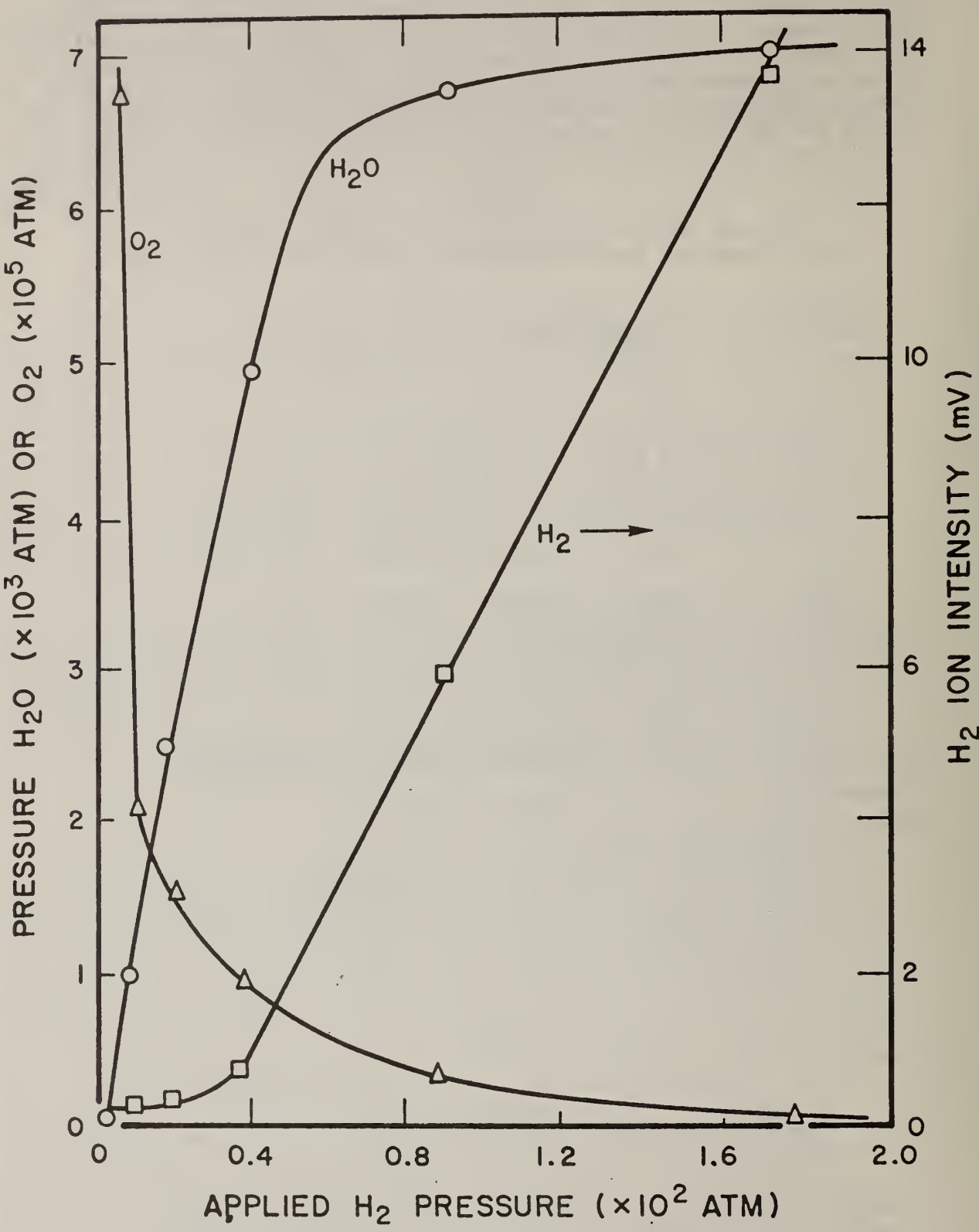

1. Response of K_2 slag system to added H_2, showing conversion of slag O_2 to H_2O. Conditions, 1655 K temperature, 0.18 atm N_2 carrier gas pressure and capillary nozzle.

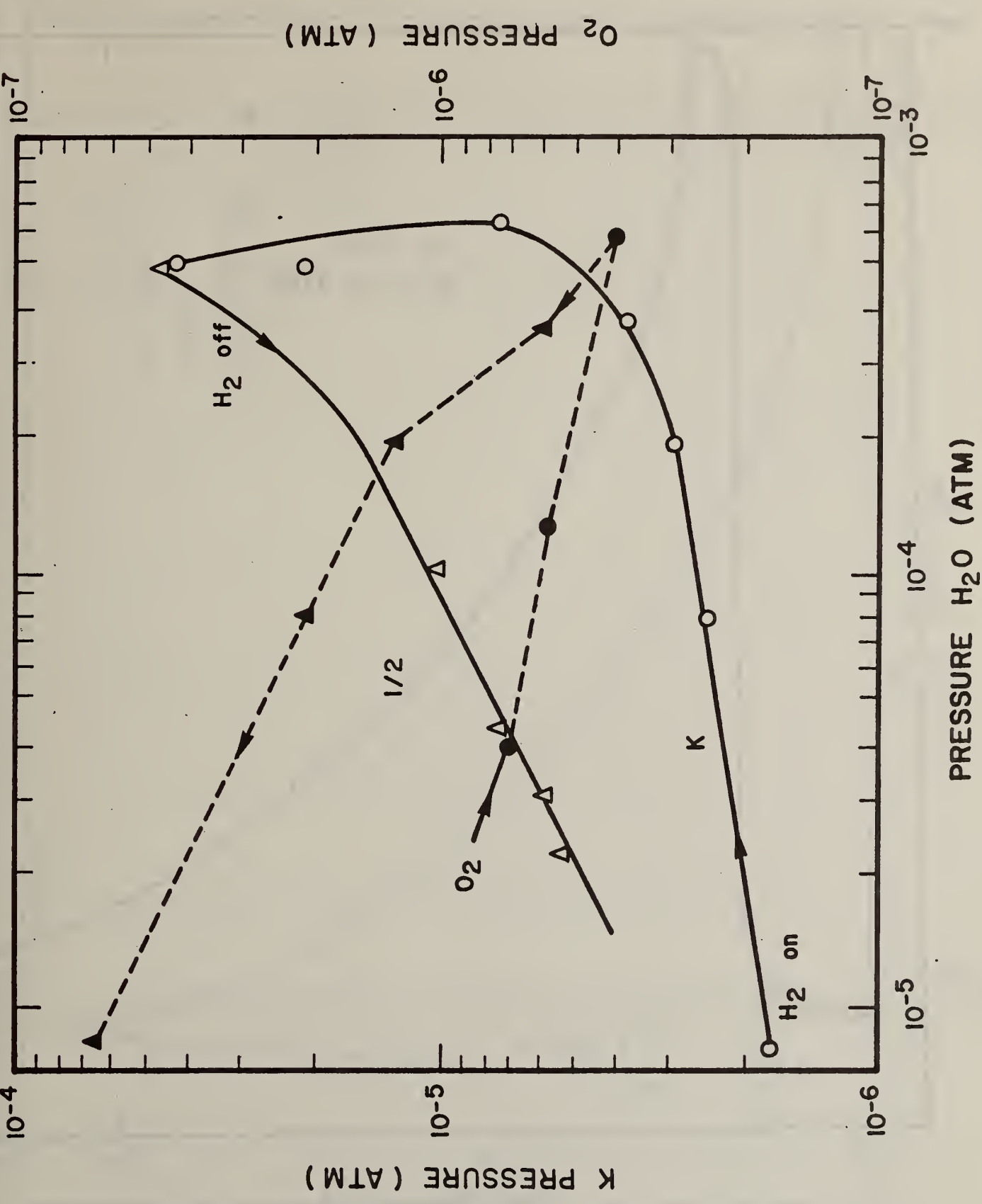

2. K-pressure (open symbols) and O_2 pressure (closed symbols) variation with H_2O for added H_2 with K_2 slag. Conditions, 1655 K temperature, 0.18 atm N_2 carrier gas pressure and capillary nozzle.

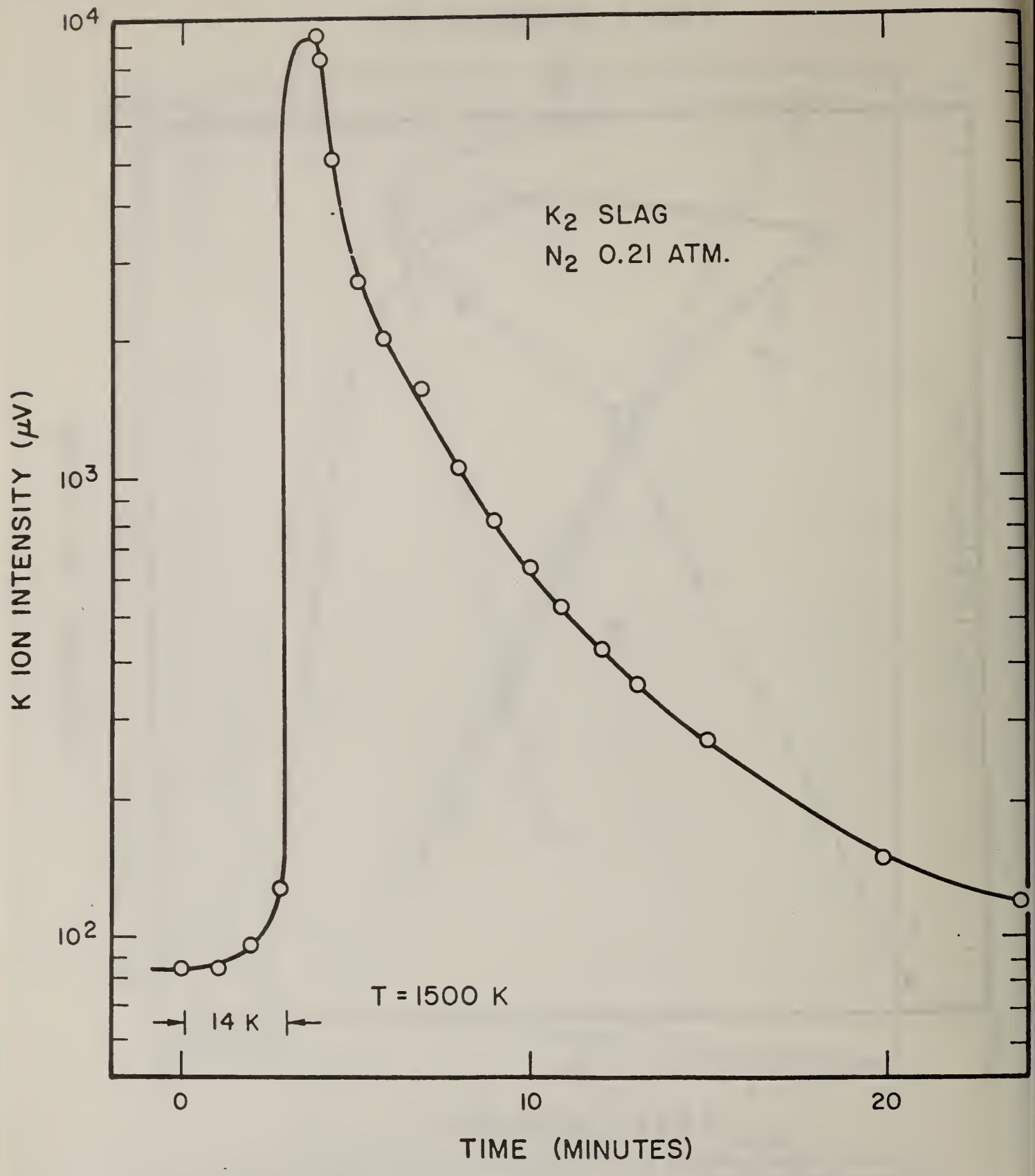

3. K-species pressure burst phenomenon expressed as K^+ ion intensity versus time, for K_2 slag. Conditions, 1655 K temperature, 0.18 atm N_2 carrier gas pressure and capillary nozzle.

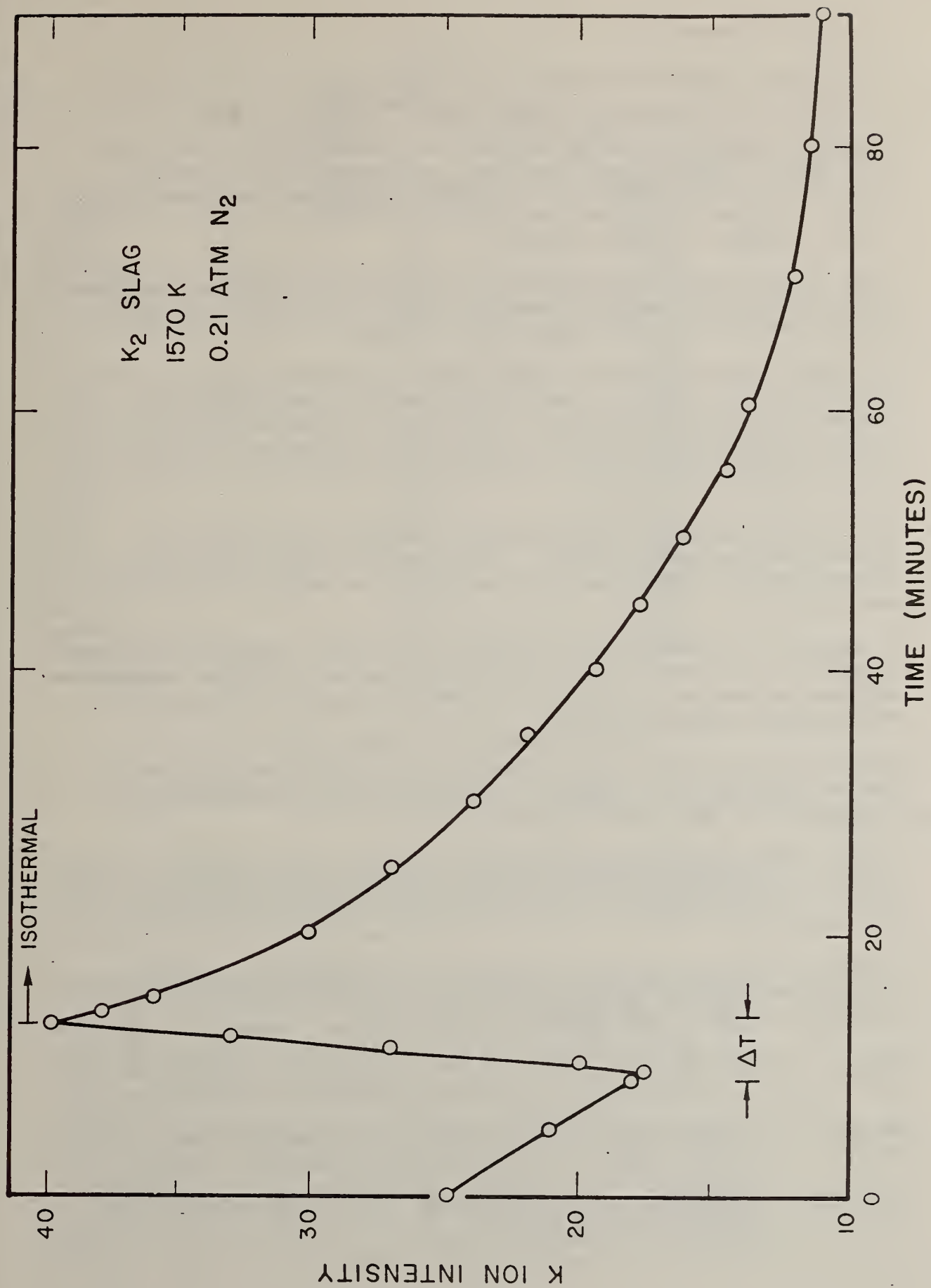

4. Typical K^+ ion intensity signal decay with time for K_2 slag. Conditions, 1570 K temperature, 0.21 atm. N_2 and capillary nozzle.

4. Failure Prevention

a. Failure Information Center (R. C. Dobbyn, W. A. Willard, 562, and W. S. Brower, 565)

Progress: During the quarter the Failure Information Center received five reports of operational experiences and materials and components failures from coal conversion pilot plants and process development units. To date, the percent contribution of failure incidents contained in the data base is shown in Table 1.

These reports have been classified and evaluated for technical completeness and accuracy. Detailed summaries of this information have been entered into the Center's computerized data bank.

The Center provided Battelle-Columbus with ten updated summaries and three hard-copy reports for possible inclusion in the DoE Newsletter feature on failure experiences. In addition, a feature article, summarizing the performance of refractory construction materials used in the CO_2 Acceptor Pilot Plant, was submitted to Battelle for publication in the October, 1979 issue.

The Failure Information Center answered fourteen other requests for information from DoE contractors. In response to these, 2,764 abstracts and ten hard-copy reports were transmitted. The Center also received one visitor.

A substantial reformatting of data base entries was completed during the quarter. Completing this task will not only better facilitate information exchange and analysis but will also speed the transfer of data to the new data base management system.

Progress was also made in the preparation of the Construction Materials Handbook for Coal Gasification, a joint project with the Materials Properties Data Center at NBS (see section b).

A draft summary report on erosive wear failures in coal conversion process plants was completed by project staff and is currently in review. Several sections of a similar report on corrosion have also been completed.

Camera-ready copy of the final report on the performance of materials and components at the CO_2 Acceptor pilot plant was transmitted to DoE during the quarter. This completes the project.

Plans: Liaison with pilot plants and failure analysis laboratory staff will continue, as will work on the construction materials handbook.

Review of the draft report on erosive wear will be completed and completion of the draft report on corrosion failures is also scheduled.

The regular information and data gathering, analysis and dissemination activities of the center will continue.

Table 1

FAILURE INCIDENTS IN COAL CONVERSION SYSTEMS

PROCESS	NO OF INCIDENTS	PERCENT
Bigas	16	3.61
BMI	35	7.91
Carbonate	5	1.13
Clean Coke	27	6.10
CO_2	52	11.76
CPC	1	0.22
Cresap	20	4.52
Exxon	3	0.67
GFETC	2	0.45
Hygas	45	10.18
Letc	3	0.67
Lignite	18	4.07
Metc	13	2.94
Misc.	15	3.39
Petc	2	0.45
SRC	22	4.97
SRC-W	17	3.84
Synthane	114	25.79
Synthoil	2	0.45
Westinghouse	30	6.78

Total Number of Incidents = 442

b. Materials Properties Data Center (H. M. Ondik, T. A. Hahn, and A. Perloff, 565, and I. J. Feinberg, 562)

Progress: The Data Center staff has continued normal operation along with work on the Construction Materials Handbook for Coal Gasification and the paper on the Current Status of Materials for Open-Cycle MHD Power Generation.

During the quarter we received responses from computer vendors to the questions raised in our technical evaluations of their proposals for computer services. Two of the nine vendors who submitted proposals have withdrawn from competition since they could not meet our requirements. The other seven vendors have responded satisfactorily and are eligible to participate in benchmark testing sessions, although conferences had to be held with two vendors to verify their ability to comply with the specifications. The benchmark base, containing some eighty data entries and a list of the types of operations to be performed, has been prepared and delivered to the Commerce ADP procurement group for distribution to the vendors. Benchmark test sessions will be scheduled by the Commerce ADP management.

Plans: It is expected that the Center staff will be occupied chiefly with the benchmark test sessions and evaluation of the results during the first portion of the next quarter. If all goes smoothly, this next quarter should see the establishment of a contract for a computer vendor's service. Draft sections of the MHD paper and further sections of the gasification handbook will be delivered.

5. Creep of MHD Refractories (N. J. Tighe, C. L. McDaniel, S. M. Wiederhorn, 562.00)

Progress: Work during this quarter concentrated on evaluating the refractory designated Corhart RFG, a rebonded fused grain chrome spinel. Specimens received from Harry Townes at Montana Tech were (1) cores cut from bricks used in the test rig and (2) sections of refractory brick removed from the test rig after a test run of 250 hours.

Experimental Procedure: The cores were machined into creep specimens three inches long with reduced cross section 1/2 inch in diameter and 1 inch long. These specimens were tested at 1400, 1500 and 1600°C in the deadweight creep apparatus. Measurements were made of the swelling during exposure at 1400, 1500, and 1600°C using cylinders 1/2 inch in diameter by one inch long. Changes in structure as a result of heating were monitored by X-ray diffraction.

The brick sections were examined using light microscopy and scanning electron microscopy. Phases were identified by X-ray diffraction and through energy dispersive X-ray analysis (EDAX) in the scanning electron microscope.

Results: The as-received RFG refractory consists of a Cr rich and an Fe rich spinel solid solution plus MgO. After heating at 1400°C, or above the material equilibrates to a single spinel plus MgO. This oxidative phase change is accompanied by a weight loss and a swelling of the specimen. The measured changes are shown in Table 1.

Table 1. Dimensional Changes During Heating of Cr-Fe Spinel Refractory RFG.

Temperature °C	Time hr	Length % Change	Diameter % Change	Weight % Change
1400°C	23	+0.3	+0.2	-0.6
1500°C	26	+0.3	+0.4	-0.6
1600°C	18	+0.2	+0.2	-0.9

Some of the weight loss can be attributed to volatization of the material. Some swelling could be attributed to void growth during heating as well as to the phase changes.

The RFG cores exhibited considerable creep at 1400, 1500 and 1600°C. Examples of the deformation are shown in figure 1 which shows (a) an as ground core (b) a specimen after 133 hours at 92 psi which crept 8.4% and (c) a specimen after 63 hours at 51 psi which crept 9.1%. These loads are heavier than those which might occur during service and were used to accelerate the deformation rate.

The brick specimens were taken at different positions in the air preheater stack at Montana. Interaction with the coal slag was evident visually on all specimens. The scanning microscopy and EDAX measurements are not complete at this time but with these techniques the slag penetration could be tracked easily in the specimens. The powder diffraction analysis showed that the type of phase transformations observed in the creep specimens occurred in specimens in the stack. The complete analysis of both sets of specimens will be presented in a later report.

Plans: The creep testing and analysis of exposed specimens of the chrome-iron spinel refractory will be completed during the coming quarter. Specimens of the magnesia-rich, alumina spinel brick (Corhart) X-317 have been machined and will be tested in creep and examined microscopically.

The furnace control system has been ordered and should be delivered in 4-5 months so that the long time creep tests can be started in early 1980.

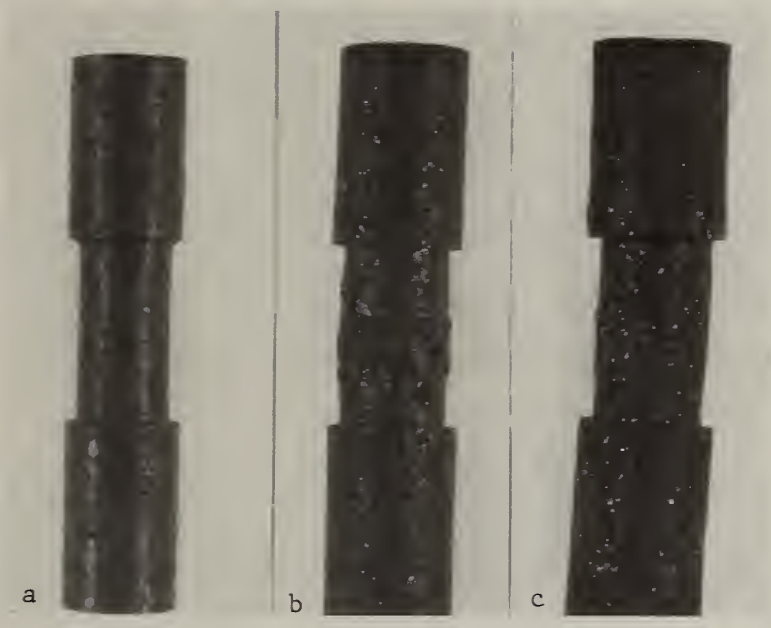

Fig. 1. Refractory (RFG) specimens from creep tests (a) as received (b) 1500°C, 133 hr, 92 psi, 8.4% deformation (c) 1600°C, 63 hr, 51 psi, 9.1% deformation.

Task 6: Electrical Transport Mechanisms in Slag Associated with Electrochemical Degradation of Insulator and Electrode Materials
(W. Hosler, T. Negas)

Progress:

a. Electrical Conductivity of $YCrO_3$

In the last quarterly report (April-June 79), a discussion of the proposed conductivity mechanism in $YCrO_3$ doped with a divalent metal such as Ca or Mg was given. Electrical data was also presented for both magnesia and calcia doped material as a function of temperature at several partial pressures of oxygen. It is evident from this data and from the model presented that the conductivity especially at low temperatures (1000½C to 25½C) is a strong function of the state of reduction obtained at higher temperature where oxygen diffusion is more rapid. It is desirable to know the conductivity as a function of oxygen pressure in this high temperature range not only because it dictates the conductivity magnitude in the low temperature range when oxygen diffusion is low, but also because it is probable that some part of this electrode system may be operating in the oxidation-reduction range of temperature (1200¼C to 1600¼C) in a functioning MHD generator. Oxygen pressures at the anode and cathode of a generator under load may be many orders of magnitude different.

A new batch of $YCrO_3$ doped with 5% Ca on the Y site was prepared by thermal sintering at 1700½C in an atmosphere of forming gas (5% H_2 - 95% N_2). From this piece a sample was cut and electrical contacts mounted using platinum leads attached by a special peaning process. The oxygen partial pressure in an atmosphere of forming gas is 10^{-14} to 10^{-15} atmospheres of O_2 as measured by a zirconia oxygen sensor. Partial pressures of a few parts per million (10^{-6} atmospheres) are obtainable by direct mixing of nitrogen and oxygen. In order to obtain pressures in the range 10^{-7} to 10^{-11} atmospheres O_2 in N_2 a special gas blender is used to mix forming gas, used as a carrier gas, with a 1 ppm O_2 in N_2 gas mixture used as a component gas.

Since $YCrO_3$ must be thermally sintered in a very low oxygen pressure, initial conductivity measurements were made at the corresponding low partial pressures (10^{-14} - 10^{-15} atmos O_2) used in the sintering process. An initial soak temperature was chosen as 1300¼C. The conductivity increased with time for the first 45 minutes (data points taken at 5 minute intervals) and then monatonically decreased over the next 6 hour period when a new soak temperature was selected. One would expect that the conductivity would increase with time until an equilibrium value would be established. Since this material was formed at 1700¼C in forming gas (most reducing condition), the sample would oxidize slightly (thus increasing the equilibrium conductivity) at 1300¼C. The data at 1400½C showed the same anomalous effect. However, several leads to the sample became open circuit after about 7 hours at this temperature.

Upon dismantling the apparatus, it was apparent that the platinum leads had melted and portions of platinum remaining intact had become very brittle. It may be that the platinum has alloyed with chromium to form a lower melting eutectic and this together with the embrittlement due to hydrogen caused the failure. No silica was present in the system. The decrease in conductivity could also have been caused by loss of chromium by diffusion into platinum near the contacts causing an ever increasing sample resistance. The cause of this failure is under investigation using the scanning electron microscope.

The platinum in the sample holder was replaced as well as the leads to the sample. Since the highly reducing atmosphere caused the problem of platinum embrittlement and melting we decided to do the high oxygen pressure equilibration experiments next. At 1300¼C and 1400½C in air an apparent equilibrium was reached after about 30 minutes. At 1500¼C, the conductivity increased nearly linearly with time for 3 hours with a total change in conductivity of about 5%. At 1600¼C, the conductivity increased about 10% in the first 40 minutes and about 50% in the next 50 minutes. While one would expect an increase in conductivity under these conditions, it is reasonable to assume that the rate of increase would diminish with time. Other effects must be present and these too are under investigation.

b. Corrosion of $YCrO_3$ in Slag

In the last quarterly report, an experiment on the electrochemical effects at 1343¼C on yttrium chromite in contact with a high iron content slag with 20% K_2SO_4 added was described. Figure 1 shows the boundary between the anode $YCrO_3$ (.05 Mg) (light grey) and the slag (dark) and Figure 2 shows a portion of this join at a magnification of 800X; the $YCrO_3$ is on the right. The grain structure in the bulk material is identical to that of the original in a tested sample. Figure 3 shows the same join area at a magnification of 1600X. The dark diagonal stripe at the lower left is the $YCrO_3$ - slag void and is caused by the difference of expansion of the two materials on cooling the test cell. Figure 4 is a Si X-Ray map of the area shown in Figure 3 and Figure 5 is a dual spectra of elements of different zones in the $YCrO_3$ just inside the void area. Note the three distinct zones labeled 1, 2, and 3 in Figure 3. Zone 3 is the bulk $YCrO_3$ and is undisturbed. Zone 1 is a reaction layer formed at the anode surface of an FeCrAl spinel without silica (see Figure 4 and lower spectra of Figure 5). Zone 2 is a densified area of Fe, Cr, Al, but high in silica with some yttria which may act as a protective layer in the cell. (Upper spectra, Figure 5) The usual silica rich layer in the near electrode slag was evident (Figure 4). The reaction layer (Zones 1 and 2) penetrated about 0.03mm into the $YCrO_3$ material.

The cathode reaction was greater. The attack zone is approximately 1.2mm into the sample. Figure 6 is a micrograph at 40X showing this attack zone (upper portion) and its relationship to the undisturbed sample. Figure 7 is a micrograph at 800X of a portion of this uniform

attack zone with Figures 7a and 7b showing the K and Ca map of this area. Potassium penetrated into the yttrium chromite with pullout of the perovskite grains of considerably smaller size than those of the original material. Unfortunately, the slag tended to pull away from the cathode electrode so that the cathode electrode analysis is limited in scope.

This test was carried out at 1343°C where the slag is molten and of adequate conductivity. Anode attack was minimal but still present. More tests should be made at lower temperatures where slag conductivity is still adequate (see next section) but where the narrow reaction zone may be diminished or eliminated. The cathode reaction zone may also be reduced if the slag temperature is lowered at the boundary, but with the slag still remaining in the high conductivity regime.

c. Slag Electrical Conductivity

The electrical conductivity data for Eastern Bow NH slag without added potassium was presented in the previous quarterly report. In this quarter, measurements were made on this same slag (analysis Table 1, page 39 QR Apr-June, 1979) but with 20% K_2SO_4 added to the melt. In the experimental procedures of loading the crucible with the slag, bubbles sometimes form in the melt. Much time may be wasted making measurements on a crucible containing a bubble in a critical area. Because of the difficulty, each crucible is now radiographed prior to contacting to make sure no bubbles remain in the bulk melt. Figures 8, 9 and 10 show a series of radiographs taken to show this effect. Figure 8 shows the crucible after being heated to above the slag melting point in a RF furnace after being filled with chunks and powders of the slag raw material. Figure 9 shows the contacted crucible; the contacts placed below the bubble. Figure 10 shows the same crucible after being held at 1500°C for 5 minutes in a muffle furnace. Note that the bubble has risen further to the crucible top and should present no difficulty in the conductivity experiment.

Electrical conductivity measurements of the potassium containing slag were made both in air and in a reduced oxygen partial pressure. However, in the latter experiment, a slight leak developed in the upper conductivity probe resulting in some slag coating on the outside surface of the crucible. This makes the validity of the data doubtful so the experiment must be repeated. Figure 11 shows the conductivity data for the potassium containing slag in air. Here, just as in the previous measurements on slag containing no added seed, the slag was quenched from some high temperature (above melting point) to 900°C where the slag is solid and then cooled slowly to about 500°C. The electrical data was taken then with increasing temperature up to the next high temperature point from which it was quenched again. Only the inverted delta (▽) data was taken with decreasing temperature. Unfortunately, the data does not fall into two distinct conductivity curves as did the data for slag without added potassium. The two curves showing the lowest conductivity are derived from quenches from the greatest difference in soak

temperatures, 1383°C and 1489°C or 1500°C. The remaining curves show higher conductivities, the relative conductivity decreasing with decreasing soak temperatures. The quench times are given in Table 1 and are listed in sequential order as the data was taken from day to day.

Soak temp.	Quench time (min.)
1500°C	21.0
1440	19.0
1408	20.0
1383	20.0
1489	23.5
1420	21.0

In contrast to the data on slag containing no added potassium, all this data showed strong polarization effects at all temperatures. As explained in the previous report, the data is taken using a power supply in the constant current mode. Polarization was observed in the current carrying probes only; an increase in applied voltage with time to maintain a constant sample current. No polarization effects were observed on the conductivity probes during the measurement time which was approximately 25 seconds.

No explanation of the data can be given at this point. X-Ray diffraction measurements show little variation in crystalline content on samples quenched to duplicate the conductivity samples. Quench times with the exception of the fifth run were nearly the same. One might attribute the changes as being due to a variation of the potassium or sulfur content as the experiment continued but the last run (1420°C soak) showed a high conductivity again similar to that obtained early in the experiment for the 1440°C soak.

Plans: A study of the effect of oxygen pressure on the electrical conductivity of $YCrO_3$ - (.05 Ca) will continue. A new approach to the low pressure ($< 10^{-7}$ atmospheres O_2 in N_2) experiments will be tried in order to eliminate the reaction of H_2 and/or chromium on platinum mentioned in the text.

The effect of slag containing potassium and sulfur on $YCrO_3$ will be determined at temperatures lower than 1343°C under current carrying conditions. This decreased temperature may lessen the electrochemical boundary layer effects between $YCrO_3$ and slag.

The work on the conductivity mechanisms of slag will continue. Eastern slag containing potassium introduced as potassium sulfate will be investigated at a reduced oxygen pressure and initial experiments started to determine the conductivity process of Western (Montana Rosebud) slag with and without added potassium.

Figure 1 - Anode boundary between $YCrO_3$ (0.05 Mg) and Bow NH slag with 20% K_2SO_4 added. (100X)

Figure 2 - Anode boundary - $YCrO_3$ on right (800X)

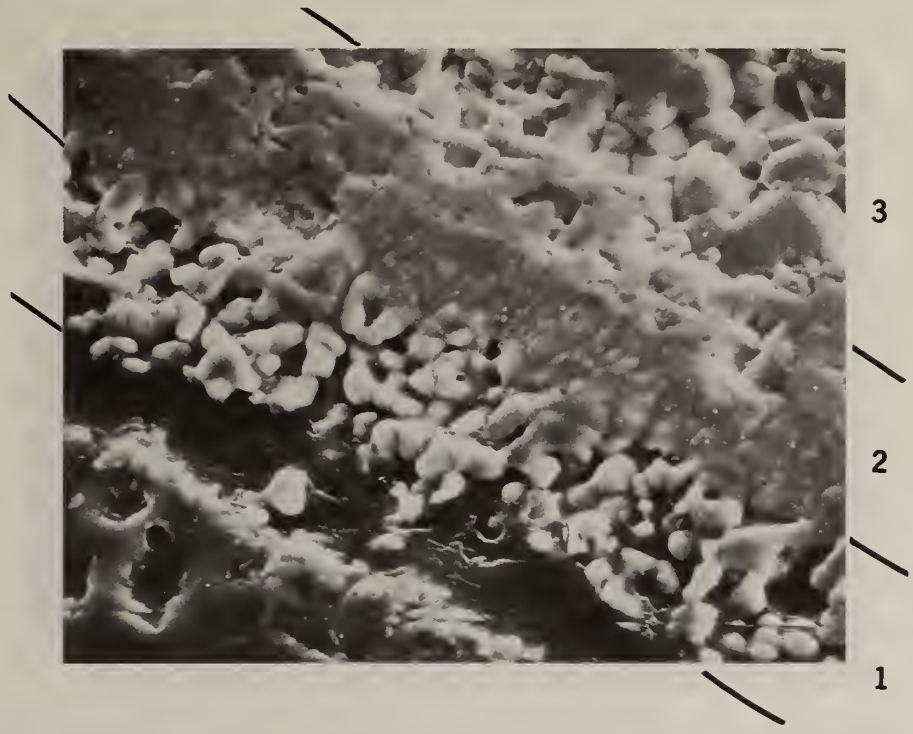

Figure 3 - Anode-slag boundary (1600X) showing three compositional zones. Dark diagonal strip on lower left is a void caused by difference in expansion of $YCrO_3$ and coal slag.

Figure 4 - Si x-ray map of area shown in Figure 3.

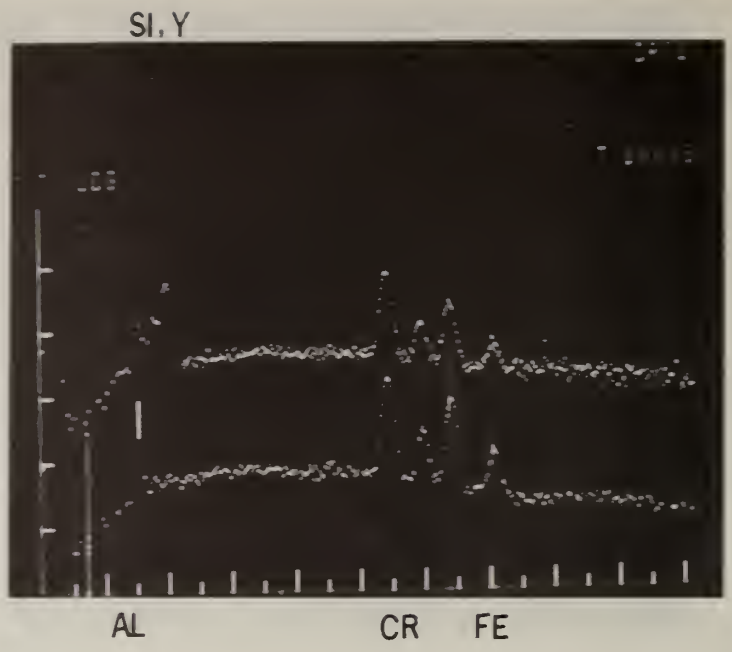

Figure 5 - Dual spectra of elements of zone 1 (lower spectrum) and zone 2 (upper spectrum) shown in Figure 3.

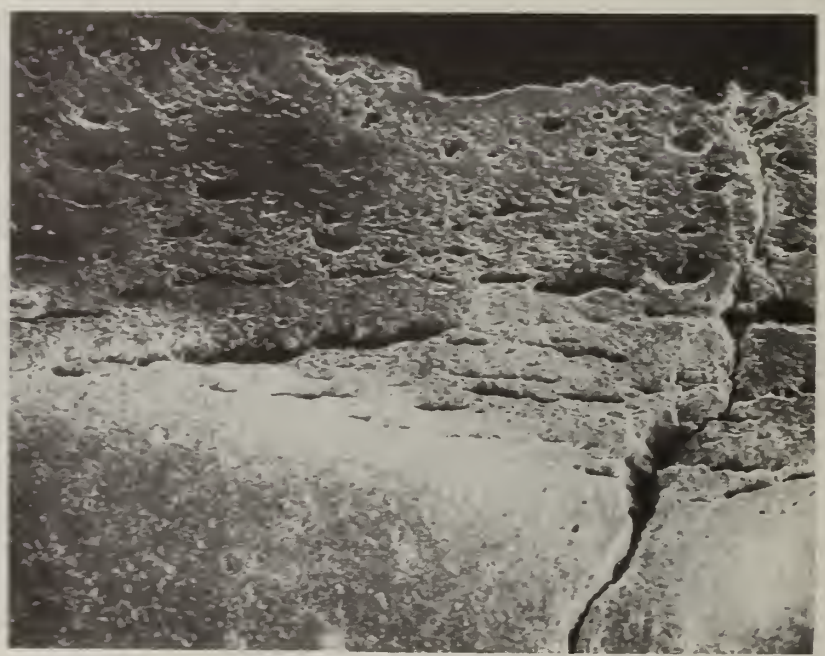

Figure 6 - Micrograph of cathode attack zone (upper half) of Bow NH slag with 20% K_2SO_4 added on $YCrO_3$ (.05 Mg). (40X)

Figure 7 - Micrograph of a section of the cathode uniform attack zone. (800X)

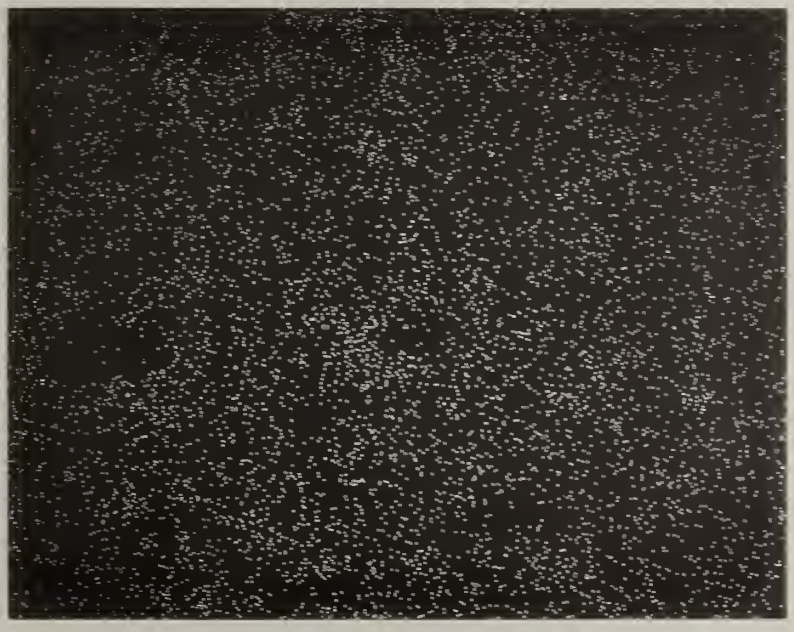

Figure 7a - Potassium x-ray map of area shown in Figure 7.

Figure 7b - Calcium x-ray map of area shown in Figure 7.

Figure 8 - Radiograph of crucible containing slag after being heated in an RF furnace to above the softening point. Note bubble formation.

Figure 9 - Radiograph of same crucible after being contacted with platinum electrodes.

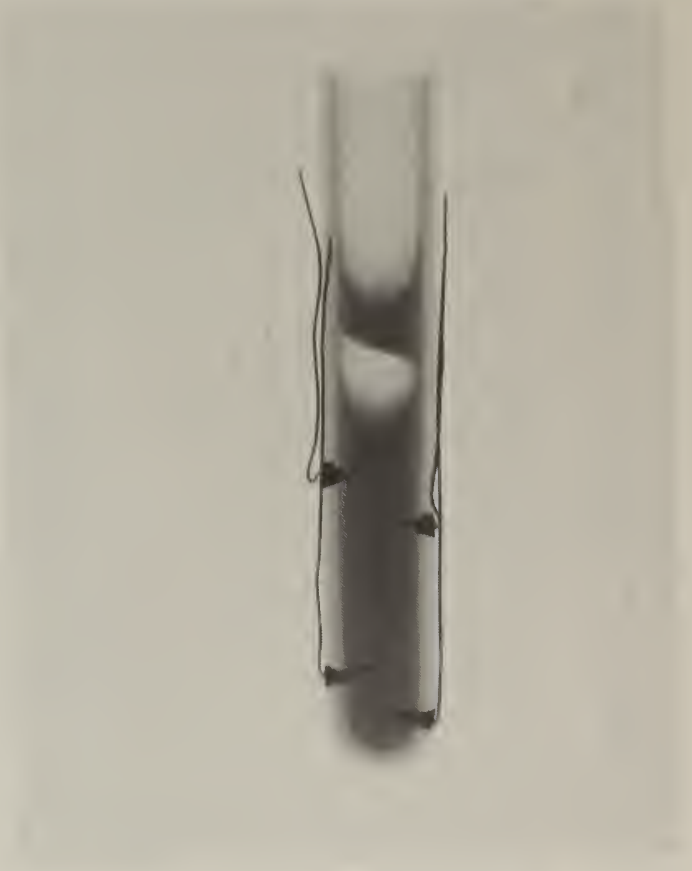

Figure 10 - Radiograph after being heated to 1500°C for 5 minutes in a muffle furnace. Note bubble is slowly rising to surface.

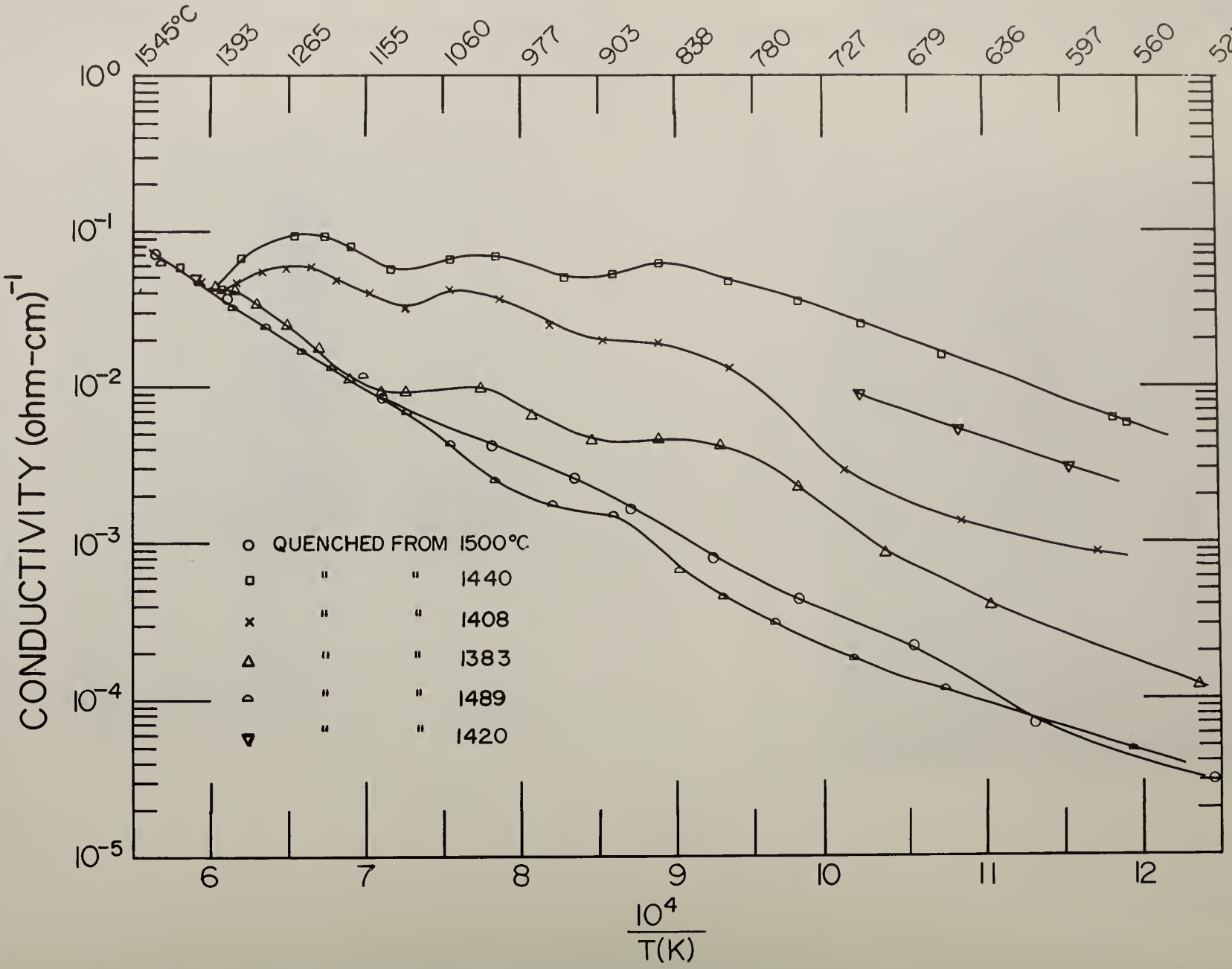

Figure 11 - Conductivity of Bow NH slag with 20% K_2SO_4 added in air as a function of temperature after being quenched to below 900°C from the soak temperatures noted in the figure.

Task 7. Corrosion of Downstream MHD Components (J. Smit, 561, and C. D. Olson, 565)

Progress: Exposure tests and SEM and EDX analysis were conducted on Type 304 stainless steel tubular specimens. The tubes were exposed to K_2SO_4 seeded propane fuel rich or oxygen rich hot gas streams. Propane and oxygen gas flow rates and ratios and gas stream color determined the gas stream condition, i.e., either fuel rich or O_2 rich. A Nernst probe was constructed to obtain O_2 partial pressure data. The probe (fabricated from a high density, closed on one end zirconia tube, platinum and platinum paste) was fired to 900°C at 2°C/mm and cooled at the same rate. It was then calibrated with O_2 and air in a static furnace system. Measurements of O_2 partial pressure in the hot gas stream were undertaken for both the fuel rich and oxygen rich conditions. In this dynamic system the probe initially withstood the thermal stresses created by bringing it from room temperature to 1000°C in minutes and also cooling it through the same interval in minutes. It also withstood heating to about 1450°C in the hot gas stream. However, the probe failed, i.e., cracked, before sufficient data was collected. At present, another design is being considered.

Gas stream temperature in the vicinity of the test specimen was maintained at approximately 1300°C while the specimen temperature in that zone was adjusted by internal air cooling to a fixed value between 400°C and 590°C. Total exposure time was four hours. During the first 25 minutes of this period the gas stream was seeded with reagent grade K_2SO_4 at a rate of about 10 grams/minute. Six specimens were tested under these general conditions. Three of the specimens were exposed to the oxygen rich gas stream with the tube temperature fixed at 400°C, 500°C, and 590°C respectively. The remaining three were exposed to the fuel rich gas stream also at 400°C, 500°C, and 590°C respectively. Each specimen was seated in the test rig with an internal Pt/Pt 10% Rh thermocouple heliarced into its wall. An external Pt/Pt 10% Rh thermocouple was placed directly into the hot gas stream slightly above and to the side of the specimen. With these strategically placed thermocouples temperatures were monitored with digital volt meters continuously during the test run. Tube wall temperatures were maintained at ±5°C.

To minimize contamination and moisture uptake in the coatings formed during the test, the specimens were removed from the test rig upon cooling down to about 40°C and potted immediately in epoxy. Metallographic specimens were prepared from sections taken at the midpoint position in the hot zone and at approximately 10 mm away from that position. The specimens were cut, ground and polished using non-aqueous media.

On each of the three Type 304 stainless steel tubes run under oxygen rich conditions a thick white, somewhat columnar deposit was formed on the upper surface of the specimens, figures 1, 2, and 3, while a thin powdery deposit formed on the remainder of the surface. The columnar deposit was approximately 2 mm thick; the powdery deposit 0.1 mm to 0.2 mm thick. SEM examination and EDX analysis of the metal-deposit interface showed what appears to be corrosion or reaction bands that increase in thickness with temperature and vary in thickness with respect to location; the thickest band being noted in the merge region of the columnar-powdery deposit at 590°C. The reaction band thicknesses range from 3 μm to 20 μm.

SEM micrograph (figure 4) is typical of the reaction bands formed in the metal-columnar deposit interface. The accompanying EDX spectra, figures 5, 6, 7, and 8 indicate a narrow band immediately adjacent to the stainless steel that is high in Ni. In this band and beyond it, going away from the metal, is a region high in Cr followed by a band high in Fe with virtually no Ni. Figure 9 shows the reaction bands in the metal interface columnar deposit powdery deposit merge zone. Figures 10 and 11 are the EDX spectra for those bands. The analysis is the same as given above. It should be noted that sulfur is markedly present in the bands adjacent to the metal showing high Ni and high Cr peaks.

Under fuel rich conditions, a thin (compared to oxygen rich conditions) less columnar type deposit formed on the upper surface of the specimens. Deposit thicknesses ranged from 0.3 mm to 0.8 mm. By contrast the powdery deposit formed on the under surface was thicker than in the oxygen rich condition, being about 0.3 mm thick, figures 12, 13, and 14. It was noted that the deposits were of a grayish cast indicating the possible presence of carbon. It was also observed that with an increase in specimen temperature the upper deposit appeared to thin, the merge region of the upper deposit with the powdery deposit appeared to descend and the powdery deposit appeared to increase in thickness. Again the metal deposit interface showed what appears to be corrosion or reaction bands that increase in reaction width with temperature and vary in thickness with location. These reaction bands range in thickness from 7 μm to perhaps 160 μm. SEM micrographs, figures 15 and 16, taken at a metal-columnar deposit interface show two distinct reaction sub-bands. EDX spectra on this region, figures 17, 18, 19, 20, 21, and 22 show high Cr peaks in the sub-band immediately adjacent to the metal-deposit interface with very little, if any, Ni present. The other sub-band shows high Fe peaks with some Ni rich zones or Cr rich zones. It should be noted that high sulfur peaks are associated with the Ni rich zones and moderate K peaks in the Fe rich zones.

Plans: Specimens of Type 304 stainless steel will be evaluated by SEM and EDX analysis after exposure to K_2CO_3 + K_2SO_4 seeded fuel rich and oxygen rich hot gas streams. As with the past series, specimen wall temperatures will be held at 400°C, 500°C, and 590°C. Exposure times for these tests will be 4 hours. At the conclusion of this series, 100 hour exposure tests with seeding every 24 hours will be initiated under conditions based on the results of these tests and the previous tests.

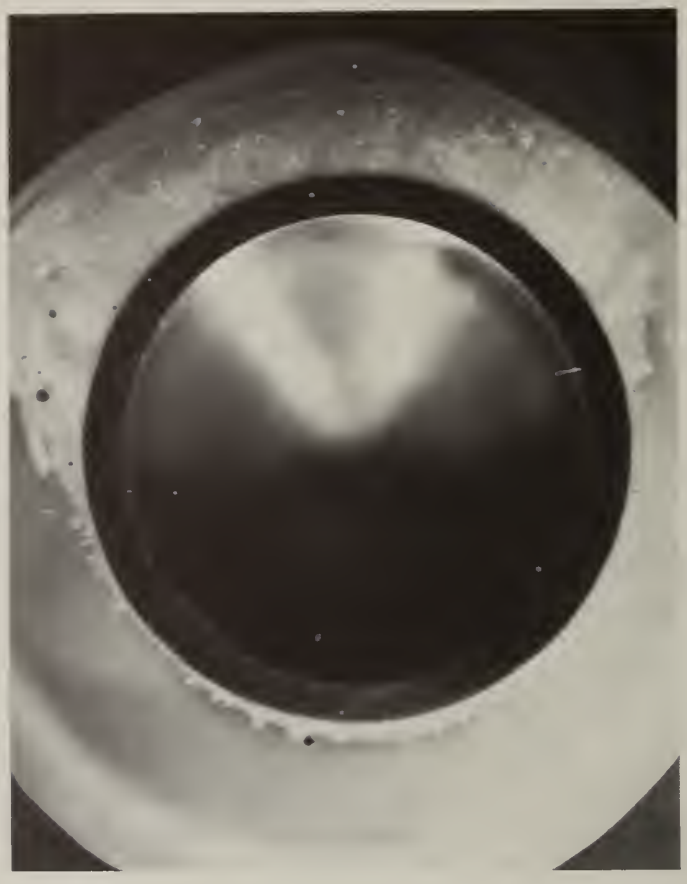

Figure 1. Section of Type 304 stainless steel tubing after exposure to K_2SO_4 seeded oxygen rich hot gas stream. Note formation of thick deposit, 2 mm, on upper surface and thin powdery deposit on lower surface. Tube temperature 400°C. 6 X.

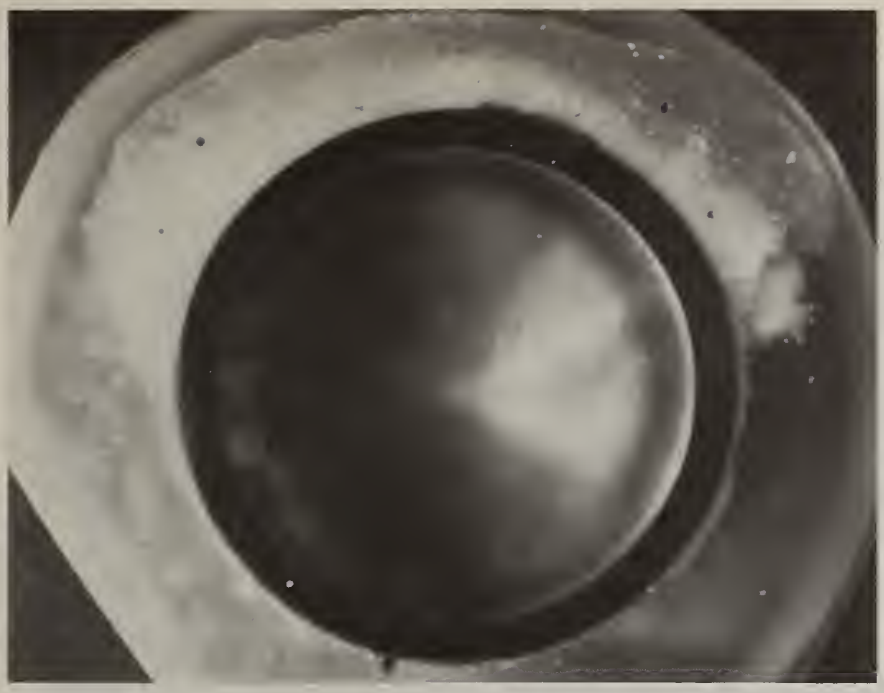

Figure 2. Section of Type 304 stainless steel tubing after exposure to K_2SO_4 seeded oxygen rich hot gas stream. Note formation of thick, 2 mm, deposit on upper surface. Tube temperature 500°C. 6 X.

Figure 3. Section of Type 304 stainless steel tubing after exposure to K_2SO_4 seeded oxygen rich hot gas stream. Note formation of thick deposit on upper surface. Tube temperature 590°C. 6 X.

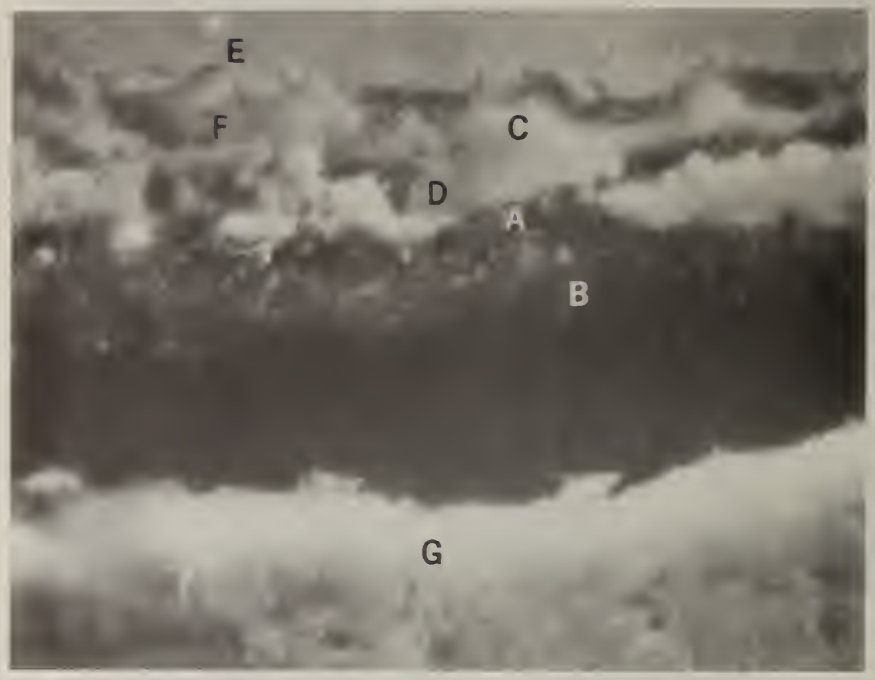

Figure 4. SEM micrograph, 4500 X of reaction bands formed in the metal-columnar deposit interface. Lettered regions correspond to labeled EDX spectra, Figures 5, 6, 7, and 8.

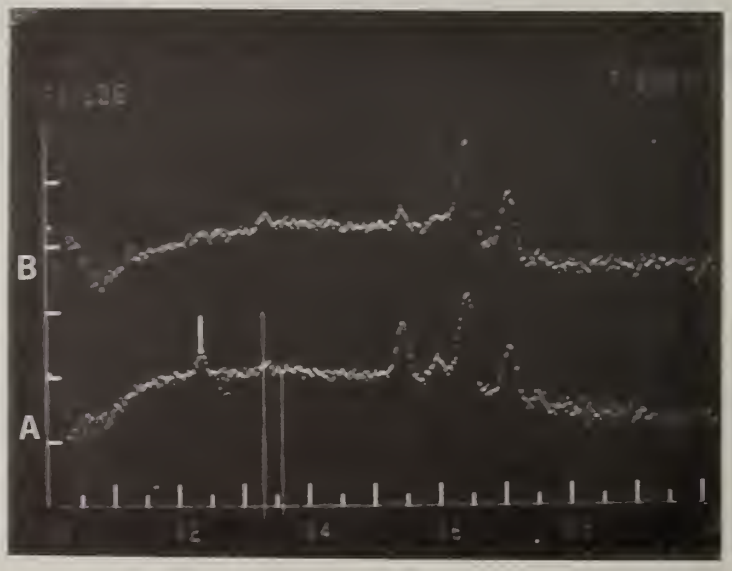

Figure 5. EDX spectra of regions A and B of Figure 4 showing absence or trace of Ni.

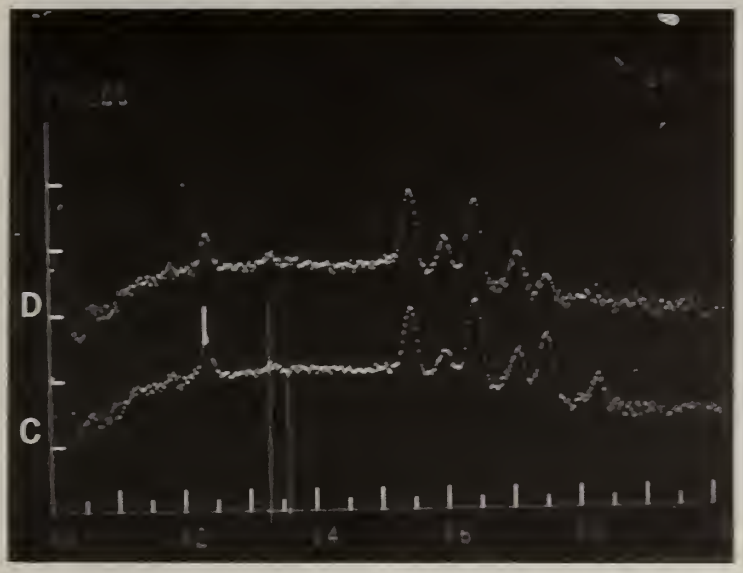

Figure 6. EDX spectra of region C and D of Figure 4 showing high Ni immediately adjacent to the stainless steel (C) and high Cr beneath it (D).

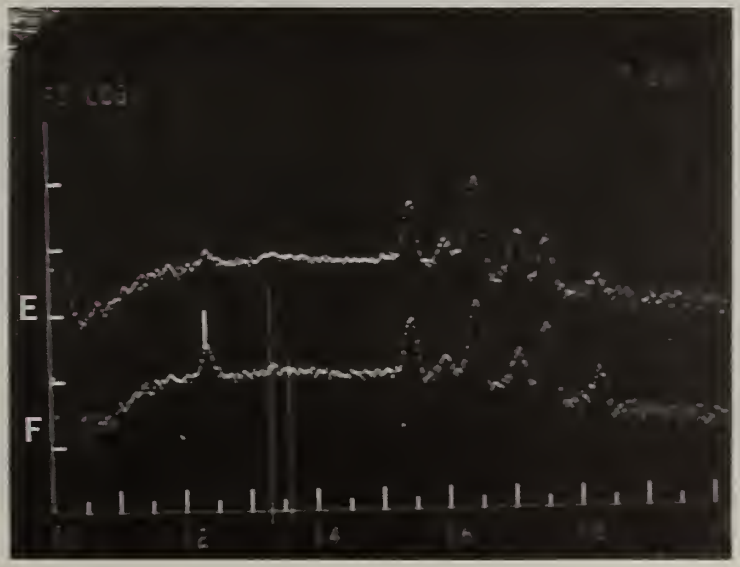

Figure 7. EDX spectra of regions E and F of Figure 4 showing stainless steel spectrum (E) and high Ni immediately adjacent to it (F).

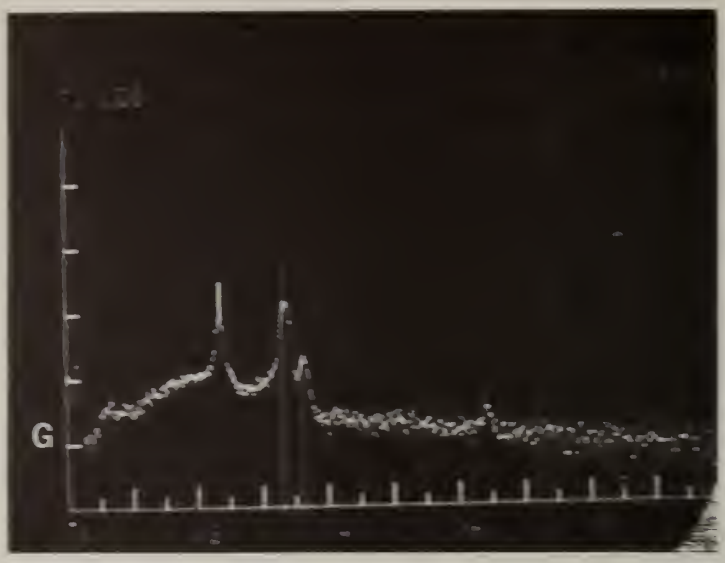

Figure 8. EDX spectrum of region G of Figure 4 showing high K and S with a trace of Fe.

Figure 9. SEM micrograph, 1800 X, of reaction bands formed in the metal interface-columnar deposit powdery merge zone, location X of Figure 3. Lettered regions correspond to EDX spectra of Figures 10 and 11.

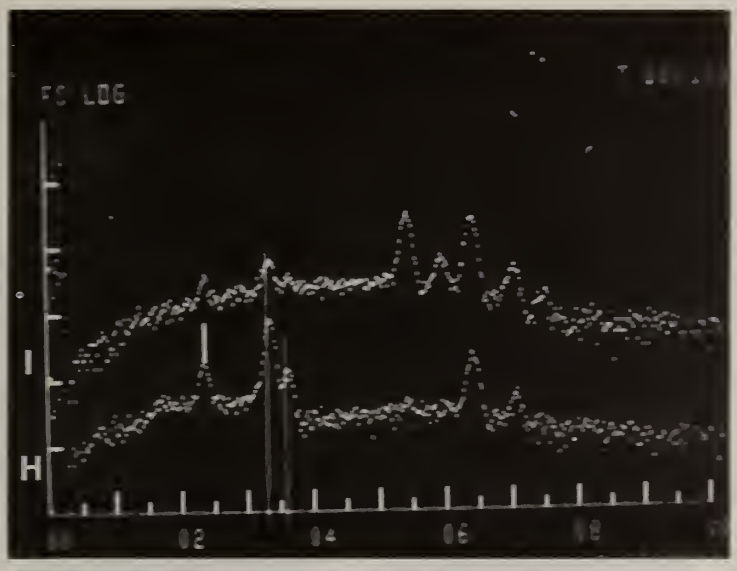

Figure 10. EDX spectra of regions H and 1 of Figure 9 showing Fe with the absence of both Cr and Ni (H) and high Cr and Fe with the absence of Ni(L).

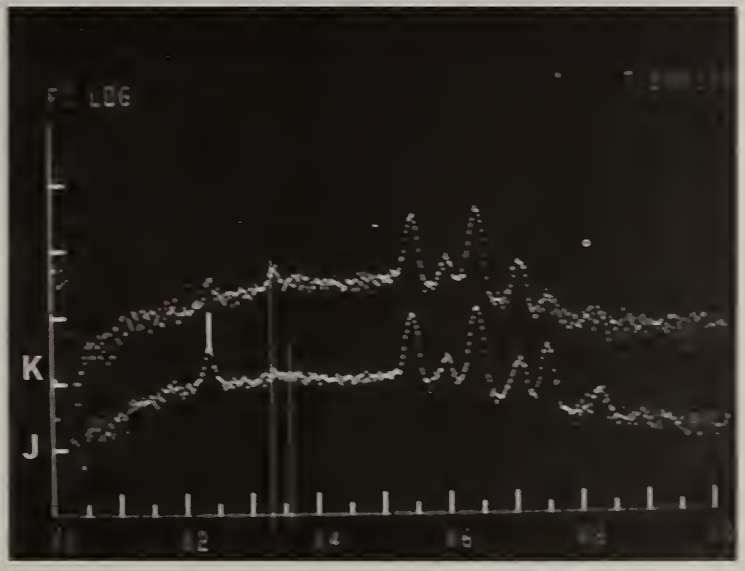

Figure 11. EDX spectra of regions K and J of Figure 10 showing high Ni and Cr with Fe (J) and high Cr with Fe and a trace of Ni (K).

Figure 12. Section of Type 304 stainless steel tubing after exposure to K_2SO_4 seeded fuel rich hot gas stream. Note formation of thin solid deposit on upper surface. Tube temperature 400°C. 6 X.

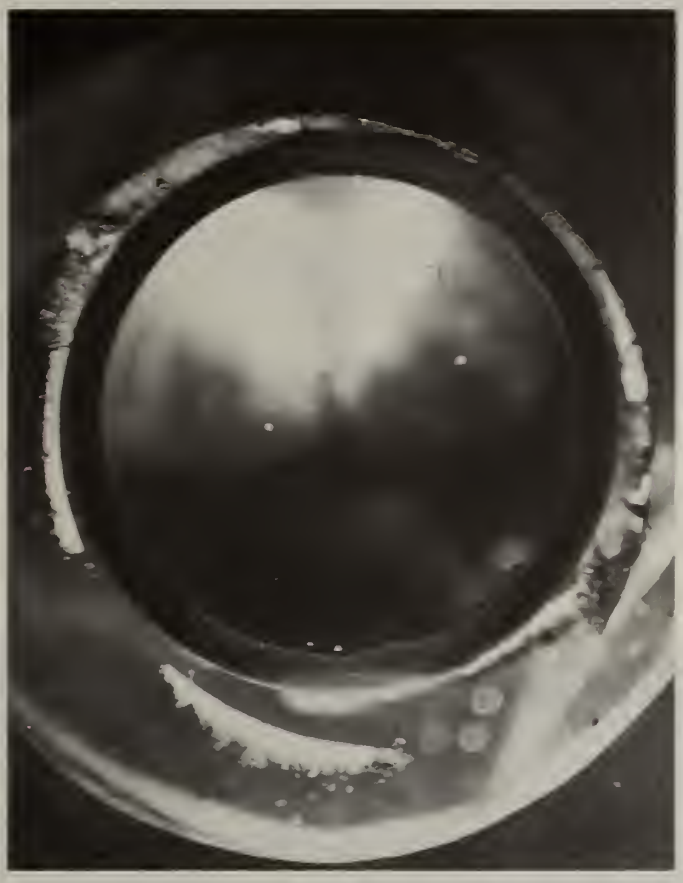

Figure 13. Section of Type 304 stainless steel tubing after exposure to K_2SO_4 seeded fuel rich hot gas stream. Note thinner solid deposit on upper surface. Tube temperature 500°C. 6 X.

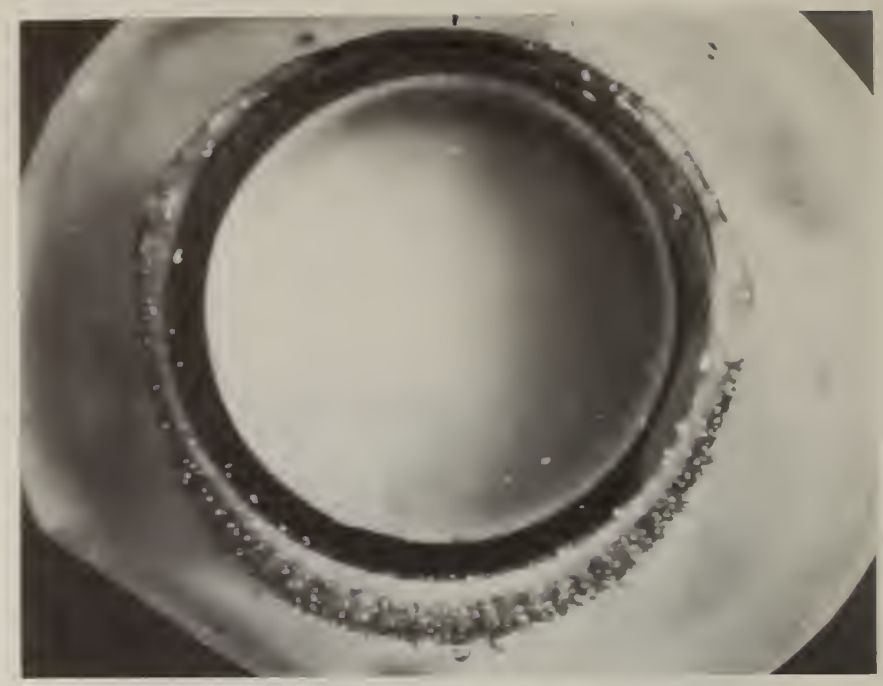

Figure 14. Section of Type 304 stainless steel tubing after exposure to K_2SO_4 seeded fuel rich hot gas stream. Note thin solid deposit, about 0.3 mm, on upper surface. Tube temperature 590°C. 6 X.

Figure 15. SEM micrograph, 190 X of reaction bands formed in the metal deposit interface of region Y of Figure 14.

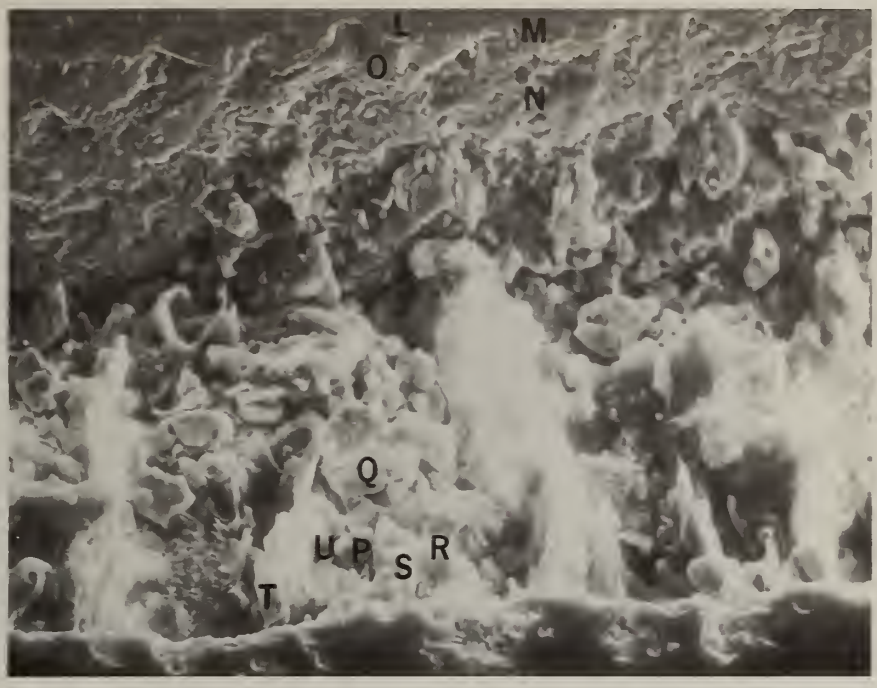

Figure 16. SEM micrograph, 450 X, of the same area as Figure 15. Lettered regions correspond to labeled EDX spectra of figures 17, 18, 19, 20, 21, and 22.

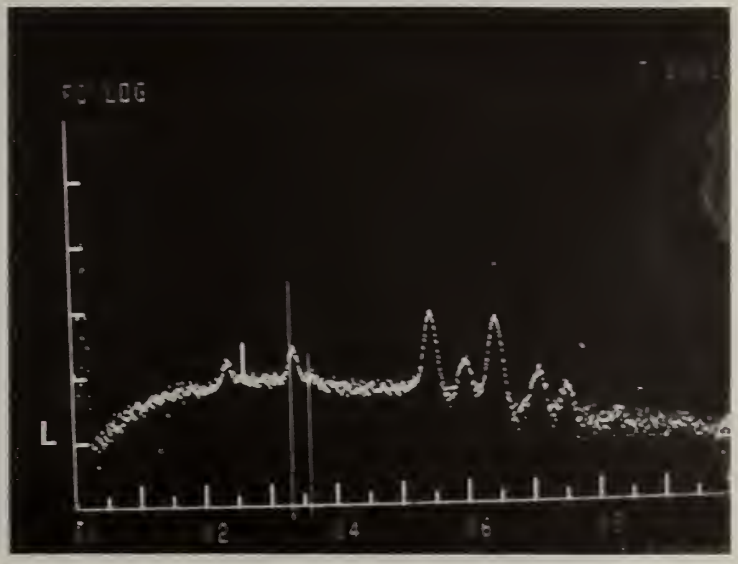

Figure 17. EDX spectrum of region L of Figure 16 showing high Cr with Fe and low Ni.

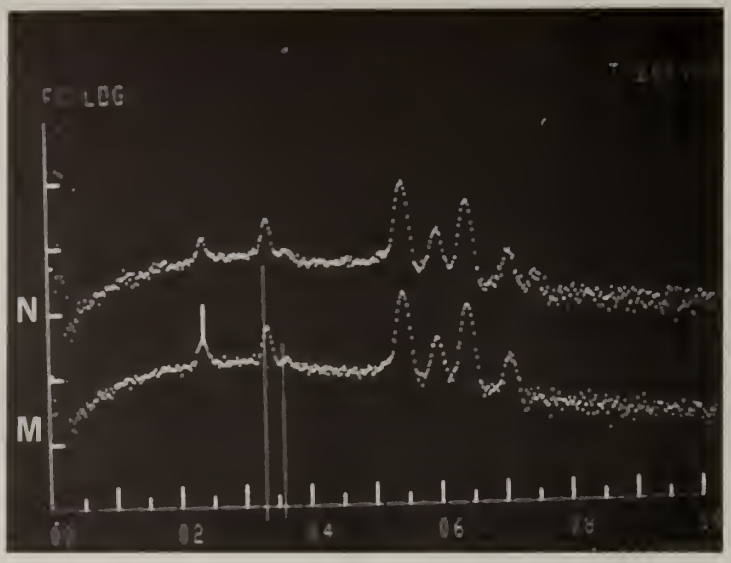

Figure 18. EDX spectra of regions M and N of Figure 16 showing high Cr with Fe and low Ni (N) and absence of Ni (M).

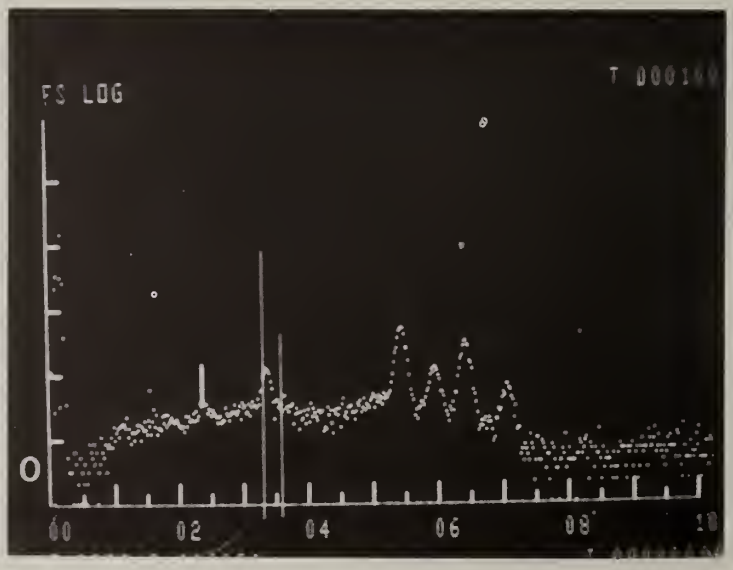

Figure 19. EDX spectrum of region O of Figure 16 showing high Cr and Fe and absence of Ni.

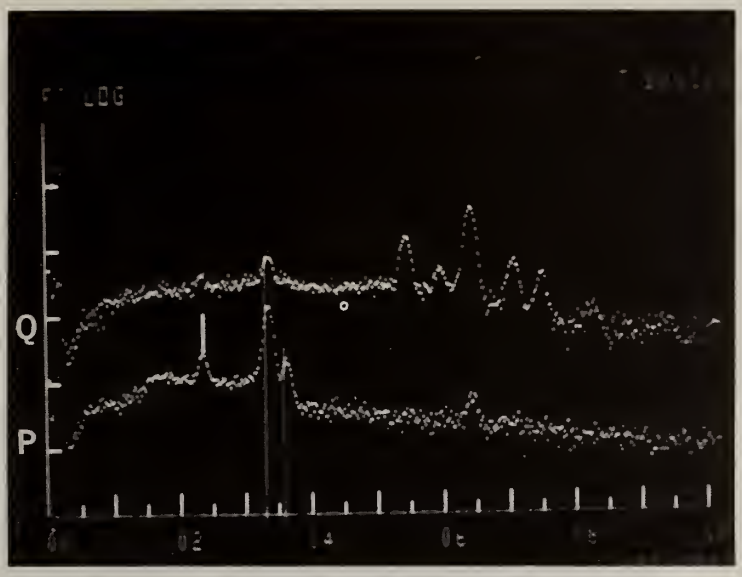

Figure 20. EDX spectra of regions P and Q of Figure 16 showing high Fe with Ni and Cr (Q) and Fe with absence of Ni and Cr (P).

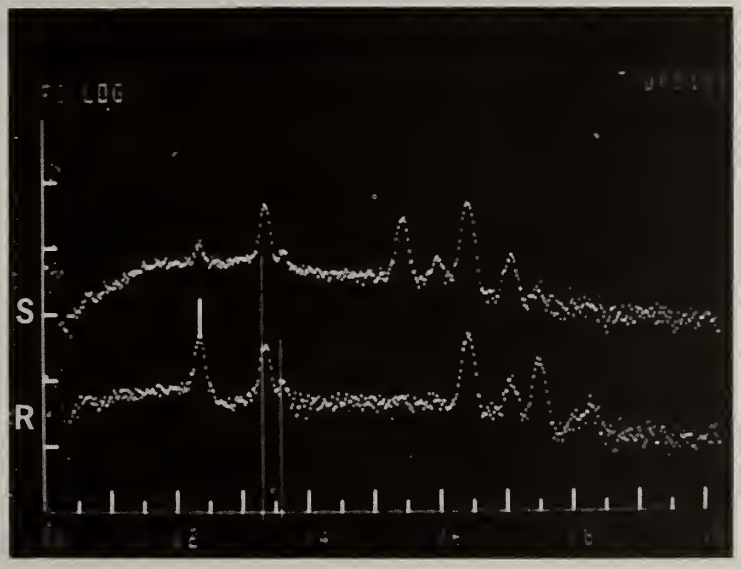

Figure 21. EDX spectra of regions R and S of Figure 16 showing Cr and Fe with a trace of Ni (S) and high Fe with Ni with no Cr, also high S and K, (R).

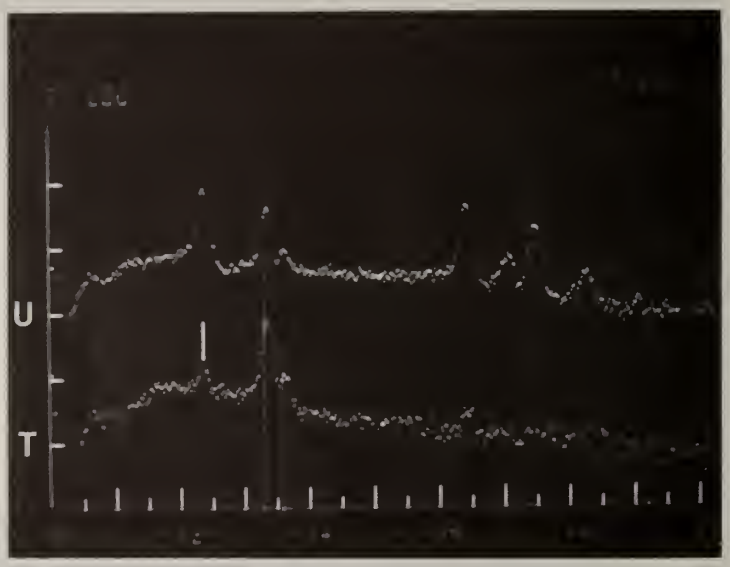

Figure 22. EDX spectra of regions U and T showing high Fe and Ni with no Cr and high S and K (U) and K and S with a trace of Fe (T).